JTTEE5 20:21–27
DOI: 10.1007/s11666-010-9560-6
1059-9630/$19.00 © ASM International

Modeling of the Plasma Flow and Anode Region Inside a Direct Current Plasma Gun

Rodolphe Bolot, Christian Coddet, Alain Allimant, and Dominique Billières

(Submitted April 29, 2010; in revised form July 29, 2010)

This study is devoted to the modeling of the arc formation in a direct current plasma gun newly commercialized by Saint-Gobain Coating Solutions (Avignon, France). The CFD computations were performed using the FLUENT code. The electromagnetic coupling was implemented on the basis of a three-dimensional model using additional scalars for the electromagnetic equations and user-defined functions to set up the problem. Whereas most of earlier models include the arc region only, the CFD domain was extended to the gas injection region (i.e., upstream part of the gun, including the gas diffuser), thus allowing a better description of the swirl injection on the plasma flow. Similarly, whereas numerous earlier works include the fluid domain only, the present model takes the fluid/solid coupling problem in the anode into account. In particular, the thermal and the electromagnetic equations are solved not only in the fluid parts but also in the tungsten and copper parts of the anode. This change was found to be important because the internal surface of the anode is no more a boundary of the domain. Thus, its temperature (and electric potential) becomes variable and is thus not necessarily imposed. Finally, the implemented model provides interesting results describing the arc behavior inside the plasma gun.

Keywords CFD modeling, DC arc, MHD model, plasma gun

1. Introduction

Important efforts have been undertaken during the last 12 years for the conception of new generation plasma torches. Multiple cathode systems such as the Triplex gun from Sulzer-Metco (Winterthur, Switzerland) (Ref 1, 2) or the Axial III system from Mettech (North Vancouver, Canada) and multiple anode torches such as the Delta gun from GTV (Luckenbach, Germany) have been commercialized. The main benefits of this new generation of torches concern (1) their ability to provide an improved stability of the arc and (2) their elevated power allowing increased deposition rates.

Saint-Gobain Coating Solutions, a business unit of Saint-Gobain group, is present as provider of thermal spray equipments and materials (ceramic powders, Rokide rods, flexible cords, flame spray guns, plasma spray, and PTA equipments). A new plasma gun called ProPlasma HP was recently designed with objectives of improving its productivity and versatility. With the permanent concern to develop simple and robust solutions, the *ProPlasma HP* gun runs with a conventional plasma spray system using a single power source. The torch power can be adjusted between 30 and 65 kW, allowing deposition rates three or four times higher than conventional plasma torches by using up to six different powder injectors. This new gun is suitable for a wide range of thermal spray applications including dense wear-resistant coatings or porosity controlled TBCs. Besides, the torch also presents a better arc stability in comparison with other single cathode guns, thus allowing improved deposition efficiencies and electrode life time. The *ProPlasma HP* gun is also suitable for long-term spray operation at more than 55 kW and has already been approved for spraying most materials such as ceramics, metals, and carbides. Moreover, it can be implemented on any existing plasma equipments.

In this study, a CFD model was developed to investigate some operating conditions of the torch. The major objectives were to achieve a better knowledge of the plasma flow inside the gun, and understanding of the arc behavior. The final model could allow testing the influence of the main thermal spray parameters such as the plasma gas flow rates or electric arc current intensity. The model will also be able to consider the main torch design parameters (swirl type or straight gas injection, electrode shape and positioning, anode diameter, design of the cooling circuit, etc.).

The state of development of the model will be presented in this article. In fact, different steps were considered: in particular a two-dimensional (2D) stationary model was first established and presented during the ''Rencontres Internationales de Projection Thermique'' (RIPT, Lille,

This article is an invited paper selected from presentations at the 2010 International Thermal Spray Conference and has been expanded from the original presentation. It is simultaneously published in *Thermal Spray: Global Solutions for Future Applications, Proceedings of the 2010 International Thermal Spray Conference*, Singapore, May 3-5, 2010, Basil R. Marple, Arvind Agarwal, Margaret M. Hyland, Yuk-Chiu Lau, Chang-Jiu Li, Rogerio S. Lima, and Ghislain Montavon, Ed., ASM International, Materials Park, OH, 2011.

Rodolphe Bolot and **Christian Coddet**, University of Technology of Belfort-Montbéliard, LERMPS, Site de Sévenans, 90010 Belfort Cedex, France; and **Alain Allimant** and **Dominique Billières**, Saint-Gobain Coating Solutions, Avignon, France. Contact e-mail: rodolphe. bolot@utbm.fr.

France, December 2009) (Ref 3). This 2D model was found to be useful to implement most of the required user-defined functions written in C language. The electromagnetic coupling was implemented by including a diffusion-type equation for the electric potential as suggested for example by Murphy and Kovitya (Ref 4). Nevertheless, the major difference with the model of Murphy et al. is that Murphy applied a numerical integration technique to deduce the θ component of the magnetic field from the current density, whereas the axial component of the magnetic vector potential was solved in our 2D model.

Similar 2D models incorporating an electromagnetic coupling are commonly applied especially to investigate transferred arcs (Ref 5, 6). For non-transferred plasmas, Li and Chen (Ref 7) considered a three-dimensional (3D) stationary model and Bhuyan and Goswami (Ref 8) used 2D and 3D stationary models to study DC plasma torches. A recent 3D model implemented in FLUENT was also suggested by Selvan et al. (Ref 9).

However, the unstable behavior of the arc formed between the cathode and the anode was investigated in numerous experimental studies (Ref 10-15). Significant voltage fluctuations are always noticed and Nogues et al. (Ref 16) showed that two different torches may result in different voltage fluctuations.

The operating conditions were thus classified in different modes (Ref 17). The steady mode is characterized by negligible voltage fluctuations and a fixed position of the arc root over the anode, but it is not desired for thermal spray applications due to the rapid destruction of the anode that would take place. The takeover mode is characterized by almost periodic fluctuations: it can be obtained using a swirl injection of the gas, providing a regular motion of the arc root on the anode surface. It is the most desirable mode, but may be obtained for moderate currents and gas flow rates only. Moreover this mode is difficultly reproducable with argon–hydrogen plasma gas mixtures. The restrike mode is certainly the most common mode encountered during thermal spraying applications with a DC gun and is characterized by large quasi-periodic fluctuations of the voltage and a very unstable behavior of the arc. It consists in successive extinctions and reattachments of the arc: the voltage increases while the arc is dragged downstream, then a closer new attachment occurs, and so on.

Recently, the arc dynamics was studied by Trelles et al. (Ref 17, 18), who developed a 3D transient model that seems to be among the most advanced ones at the present time. Moreau et al. (Ref 19) also developed a 3D transient model to study the restrike mode and used nonconventional boundary conditions at the cathode tip and the anode surface (i.e., fixed electric potential on both instead of a current density profile at the cathode tip). These two groups published a common paper that may be considered as the actual state of the art (Ref 20).

In this study, although the final objective is to develop a transient model able to predict the arc movement inside the torch, a stationary assumption was applied to set up the model and to check its ability to provide good predictions of the average torch voltage and of the dissipated power versus parameters. The stationary solution could be obtained by imposing an artificial electrical conductibility as discussed later. Thus, the present model is able to represent the time average values of the flow characteristics but not the arc movement inside the torch. Nevertheless, the present 3D model is more advanced than most of the previous models concerning some particular aspects. First of all, as considered by Gonzalez et al. (Ref 21) in the case of transferred arcs, the calculation domain includes the upstream components of the gun, consisting in the gas injection sleeves, the effect of which can thus be studied (i.e., straight or swirl injection of the gas mixture). Secondly, the fluid/solid coupling problem is considered and the electromagnetic and thermal equations are solved not only in the plasma region but also in the tungsten and copper parts of the cylindrical anode. The use of such a coupling within the anode was also considered by Lago et al. (Ref 22) in the case of a 2D model applied to a transferred arc. Concerning non-transferred plasma jets, a first approach of plasma/anode interactions was performed by Baudry et al. (Ref 23), but the authors did not consider a fully coupled model. With this change, the internal surface of the anode is no more a boundary of the domain at which the electric potential and temperature must be imposed. On the contrary, the surface temperature of the anode is now computed from the continuity of the thermal flux on both sides of the surface.

2. Mathematical Formulation of the 3D-Coupled Model

The present model was developed using the FLUENT general purpose CFD code commercialized by ANSYS Inc (Canonsburg, PA). The implementation of the module was based on the use of user-defined functions in C language.

The main assumptions are:

- Production of a stationary flow using an artificial electric conductive layer over a part of the anode internal surface.
- The plasma is in local thermodynamic and chemical equilibrium (i.e., the deviation from LTE in the near electrode regions is neglected).
- Quasi-neutrality is considered in the whole domain (i.e., the local amount of the positive charges equals that of the electrons).
- The plasma is optically thin.
- The flow is compressible and laminar.

In the plasma volume, the default momentum equations considered within FLUENT were let unchanged except that the Lorentz forces were added as source terms for each component of the velocity.

The continuity and momentum equations were thus considered as:

$$\frac{\partial(\rho u)}{\partial x}+\frac{\partial(\rho v)}{\partial y}+\frac{\partial(\rho w)}{\partial z}=\vec{\nabla}\cdot\left(\rho\vec{V}\right)=0 \qquad \text{(Eq 1)}$$

$$\frac{\partial(\rho uu)}{\partial x}+\frac{\partial(\rho vu)}{\partial y}+\frac{\partial(\rho wu)}{\partial z}-\frac{\partial}{\partial x}\left[\mu\frac{\partial u}{\partial x}\right]-\frac{\partial}{\partial y}\left[\mu\frac{\partial u}{\partial y}\right]-\frac{\partial}{\partial z}\left[\mu\frac{\partial u}{\partial z}\right]=\vec{\nabla}\cdot\left(\rho\vec{V}u-\mu\vec{\nabla}u\right)=-\frac{\partial P}{\partial x}+\vec{\nabla}\cdot\left(\mu\frac{\partial\vec{V}}{\partial x}\right)-\frac{2}{3}\frac{\partial}{\partial x}\left(\mu\vec{\nabla}\cdot\vec{V}\right)+F_x \quad \text{(Eq 2)}$$

$$\frac{\partial(\rho uv)}{\partial x}+\frac{\partial(\rho vv)}{\partial y}+\frac{\partial(\rho wv)}{\partial z}-\frac{\partial}{\partial x}\left[\mu\frac{\partial v}{\partial x}\right]-\frac{\partial}{\partial y}\left[\mu\frac{\partial v}{\partial y}\right]-\frac{\partial}{\partial z}\left[\mu\frac{\partial v}{\partial z}\right]=\vec{\nabla}\cdot\left(\rho\vec{V}v-\mu\vec{\nabla}v\right)=-\frac{\partial P}{\partial y}+\vec{\nabla}\cdot\left(\mu\frac{\partial\vec{V}}{\partial y}\right)-\frac{2}{3}\frac{\partial}{\partial y}\left(\mu\vec{\nabla}\cdot\vec{V}\right)+F_y \quad \text{(Eq 3)}$$

$$\frac{\partial(\rho uw)}{\partial x}+\frac{\partial(\rho vw)}{\partial y}+\frac{\partial(\rho ww)}{\partial z}-\frac{\partial}{\partial x}\left[\mu\frac{\partial w}{\partial x}\right]-\frac{\partial}{\partial y}\left[\mu\frac{\partial w}{\partial y}\right]-\frac{\partial}{\partial z}\left[\mu\frac{\partial w}{\partial z}\right]=\vec{\nabla}\cdot\left(\rho\vec{V}w-\mu\vec{\nabla}w\right)=-\frac{\partial P}{\partial z}+\vec{\nabla}\cdot\left(\mu\frac{\partial\vec{V}}{\partial z}\right)-\frac{2}{3}\frac{\partial}{\partial z}\left(\mu\vec{\nabla}\cdot\vec{V}\right)+F_z \quad \text{(Eq 4)}$$

The energy conservation equation was formulated in terms of enthalpy, using an additional scalar, whereas the temperature was reset according to the enthalpy equation. This change allows a higher flexibility concerning implementation of the plasma properties (and more particularly the specific heat).

Four additional scalars were also added for the electric potential and the three components of the magnetic potential vector. Finally, the coupling equations can be formalized as follows:

- Electric potential:

$$-\frac{\partial}{\partial x}\left[\sigma\left(\frac{\partial\phi}{\partial x}\right)\right]-\frac{\partial}{\partial y}\left[\sigma\left(\frac{\partial\phi}{\partial y}\right)\right]-\frac{\partial}{\partial z}\left[\sigma\left(\frac{\partial\phi}{\partial z}\right)\right]=0 \quad \text{(Eq 5)}$$

  in which σ is the electrical conductibility, ϕ is the electric potential, and x, y, and z stand for the components of the Cartesian coordinate system.

- Magnetic potential vector:

$$-\frac{\partial^2 Ax}{\partial x^2}-\frac{\partial^2 Ax}{\partial y^2}-\frac{\partial^2 Ax}{\partial z^2}=\mu_0 j_x=-\mu_0\sigma\frac{\partial\phi}{\partial x} \quad \text{(Eq 6)}$$

$$-\frac{\partial^2 Ay}{\partial x^2}-\frac{\partial^2 Ay}{\partial y^2}-\frac{\partial^2 Ay}{\partial z^2}=\mu_0 j_y=-\mu_0\sigma\frac{\partial\phi}{\partial y} \quad \text{(Eq 7)}$$

$$-\frac{\partial^2 Az}{\partial x^2}-\frac{\partial^2 Az}{\partial y^2}-\frac{\partial^2 Az}{\partial z^2}=\mu_0 j_z=-\mu_0\sigma\frac{\partial\phi}{\partial z} \quad \text{(Eq 8)}$$

  in which Ax, Ay, and Az are the components of the magnetic potential vector and μ_0 is the permeability of free space.

These four equations are valid in both fluid and solid parts of the calculation domain, providing that σ is set accurately in each region.

In the plasma, σ was set from:

$$\sigma=\max(0.001;\sigma(T))$$

in which $\sigma(T)$ was obtained versus temperature and plasma gas nature using the software developed in (Ref 24).

In the tungsten part of the anode, σ was estimated from (Ref 25):

$$\sigma_{WTh}=\frac{1}{2,54.10^{-14}T^2+2,3.10^{-10}T} \quad \text{(Eq 9)}$$

The above relationship was applied instead of a single constant value to take into account the possible decrease of the tungsten conductibility with the temperature increase at arc root attachment on the anode surface.

Since the electric potential drop across the overall anode was found to be low (a few mV only), a single value of the electric conductibility was used in the copper part of the anode.

Once the magnetic potential equations are solved, the components of the magnetic field may be calculated from:

$$B_x=\frac{\partial Az}{\partial y}-\frac{\partial Ay}{\partial z} \quad \text{(Eq 10)}$$

$$B_y=\frac{\partial Ax}{\partial z}-\frac{\partial Az}{\partial x} \quad \text{and} \quad \text{(Eq 11)}$$

$$B_z=\frac{\partial Ay}{\partial x}-\frac{\partial Ax}{\partial y} \quad \text{(Eq 12)}$$

And the components of the Lorentz force $F=\vec{j}\wedge\vec{B}$ are given by:

$$F_x=-\sigma\frac{\partial\phi}{\partial y}\left(\frac{\partial Ay}{\partial x}-\frac{\partial Ax}{\partial y}\right)+\sigma\frac{\partial\phi}{\partial z}\left(\frac{\partial Ax}{\partial z}-\frac{\partial Az}{\partial x}\right) \quad \text{(Eq 13)}$$

$$F_y=-\sigma\frac{\partial\phi}{\partial z}\left(\frac{\partial Az}{\partial y}-\frac{\partial Ay}{\partial z}\right)+\sigma\frac{\partial\phi}{\partial x}\left(\frac{\partial Ay}{\partial x}-\frac{\partial Ax}{\partial y}\right) \quad \text{(Eq 14)}$$

$$F_z=-\sigma\frac{\partial\phi}{\partial x}\left(\frac{\partial Ax}{\partial z}-\frac{\partial Az}{\partial x}\right)+\sigma\frac{\partial\phi}{\partial y}\left(\frac{\partial Az}{\partial y}-\frac{\partial Ay}{\partial z}\right) \quad \text{(Eq 15)}$$

Moreover, the enthalpy equation solved in the plasma region was formulated as:

$$\frac{\partial(\rho uh)}{\partial x}+\frac{\partial(\rho vh)}{\partial y}+\frac{\partial(\rho wh)}{\partial z}-\frac{\partial}{\partial x}\left[\frac{\kappa}{Cp}\left(\frac{\partial h}{\partial x}\right)\right]-\frac{\partial}{\partial y}\left[\frac{\kappa}{Cp}\left(\frac{\partial h}{\partial y}\right)\right]-\frac{\partial}{\partial z}\left[\frac{\kappa}{Cp}\left(\frac{\partial h}{\partial z}\right)\right]=Q_J-Q_R+\left(u\frac{\partial P}{\partial x}+v\frac{\partial P}{\partial y}+w\frac{\partial P}{\partial z}\right) \quad \text{(Eq 16)}$$

in which

$$Q_J = \frac{j^2}{\sigma} = \sigma\left[\left(\frac{\partial\phi}{\partial x}\right)^2 + \left(\frac{\partial\phi}{\partial y}\right)^2 + \left(\frac{\partial\phi}{\partial z}\right)^2\right] \quad \text{(Eq 17)}$$

In this equation, ρ stands for density, P for pressure, u, v, and w are the components of the velocity, h is the enthalpy, κ is the thermal conductivity, Cp is the specific heat, and Q_R is the radiative loss term which was estimated versus electron density and temperature on the basis of the work of Wilbers et al. (Ref 26). However, since the correlation was established for pure Argon, an underestimation of the radiative losses may be possible. Nevertheless, the radiative loss term being not available for each plasma mixture, the correlation provided by Wilbers et al. may be considered as a first approximation assuming that the radiative loss term of any plasma depends mainly on the electron density and temperature.

The last term ($\vec{V} \cdot \vec{\nabla} P$) was omitted in the first version of the program but is now incorporated. Since the pressure gradient along the torch axis is negative in regard of the velocity vector positive orientation, this term has a cooling effect and its order of the magnitude is given in the section of the numerical results. It represents the cooling provided by the pressure drop.

In solid parts of the domain, the energy equation is solved in terms of temperature from:

$$-\frac{\partial}{\partial x}\left[\kappa\left(\frac{\partial T}{\partial x}\right)\right] - \frac{\partial}{\partial y}\left[\kappa\left(\frac{\partial T}{\partial y}\right)\right] - \frac{\partial}{\partial z}\left[\kappa\left(\frac{\partial T}{\partial z}\right)\right] = Q_J + S_R \quad \text{(Eq 18)}$$

In the tungsten part, the thermal conductivity was set according to:

$$\kappa_{WTh} = \frac{786.5}{T^{0.2726}} \quad \text{(Eq 19)}$$

which gives 168 $W \cdot m^{-1} \cdot K^{-1}$ at 288 K.

This correlation was deduced by numerical fitting of data found in the literature.

In the copper region, a single constant value of 400 $W \cdot m^{-1} \cdot K^{-1}$ was used as first approximation.

The term Q_J represents the Joule effect in the solid parts of the domain and has the same expression as the previous one.

Concerning S_R, it represents the contribution of the radiative losses of the plasma on the heating of the solid parts. In the model, the integral of Q_R over the plasma volume was wholly redistributed in the tungsten part of the anode.

2.1 Boundary Conditions

A cross-section of the computational domain is shown in Fig. 1. The internal diameter of the torch is 8 mm and that of the tungsten insert is 10 mm. In principle, the insert is cylindrical but it was modified to avoid the formation of very flat cells at the left tungsten/copper connexion (sharp angle of the tungsten volume in reality). The anode cooling water circulates over the hollowed part of the external surface of the copper, whereas the right extremity of the anode is less cooled. The gas injection orifices are not shown in this picture but are included in the computational domain: actually, the plasma gas is injected through eight injectors which allow providing both axial and swirl components to the gas velocity. Internal connections between the different colors represent coupled boundaries which do not require additional data. Concerning the left walls in contact with the cold plasma gas flow, the enthalpy was given as that corresponding to a temperature of 288 K, except for those in contact with the cathode surface (2000 K in this case).

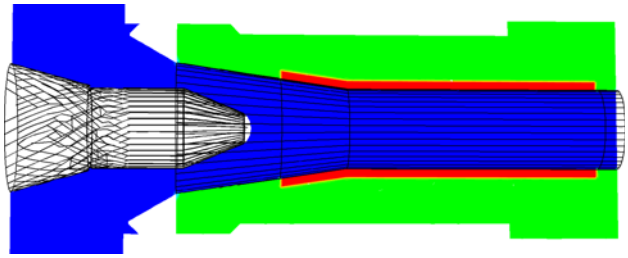

Fig. 1 View of the computational domain including the plasma region and the tungsten and copper parts of the anode

For the copper surface in contact with the cooling water, an exchange coefficient of 20,000 $W \cdot m^{-2} \cdot K^{-1}$ was considered with a water temperature of 25 °C on the opposite side of the boundary. This value of the exchange coefficient was first estimated on the basis of the use of an empirical relationship, and it was then confirmed by CFD calculations of the water flow performed separately. The electric potential was fixed to 0 V over the external circumference of the copper part of the anode. Concerning the components of the magnetic potential vector, a zero flux boundary condition was applied ($\partial Ai/\partial n = 0$) over all external surfaces except at the plasma exit for which $Ai = 0$ was used. In principle, the zero flux boundary condition could also be applied at the torch exit. Nevertheless, all components must be fixed at one point at least. We have observed that both the methods (namely $\partial Ai/\partial n = 0$ everywhere $+ Ai = 0$ in a small volume or $\partial Ai/\partial n = 0$ except at the gun exit) give similar results. Finally, the retained method is similar to that used by Trelles et al. (Ref 17).

A current density profile was used at the cathode tip. It was found from the 2D model that using a sharp profile leads to an increase of the predicted torch voltage, in comparison with the case of a constant current density (Ref 3).

Finally, the use of

$$j(r) = j_0 \exp\left[-\left(\frac{r}{0.75}\right)^5\right] \quad \text{with } r \text{ in mm} \quad \text{(Eq 20)}$$

was considered in all cases considered here. Once again, this type of current profile was taken from the work of Trelles et al. and the value of j_0 was determined so that the integration of the flux over the cathode tip surface gives 600 A exactly. In practice, j_0 is about 360 $A \cdot mm^{-2}$.

The different boundary conditions applied for all variables are summarized in Table 1. For the external surface of the anode (Sext_Anode), convection was applied for

surfaces in contact with the cooling water only. Otherwise, an adiabatic assumption was applied.

One of the most important assumption of the model was that an artificial electrical conductibility was applied over the surface of the anode along a 2 mm large and 600 µm thick line: in practice, a value of $\sigma = 5000\ \Omega^{-1} \cdot m^{-1}$ was used within this layer only if the temperature-dependant calculated conductibility is lower. This artificial conductive layer shown in Fig. 2 allowed fixing the arc root along the corresponding line to allow providing a stationary solution. From experimental results and observations made over the anode surface, the arc attachment is always positioned over the tungsten part of the anode and the damages observed on old anodes (if present) are always observed beyond the convergent part (i.e., at the beginning of the cylindrical part of the hollow anode). The positioning of the artificial conductive layer was thus performed by taking these observations into account.

For a given fluid/solid interface, the flux transferred from the plasma side to the solid side may be calculated as:

$$q = -\kappa/Cp(\partial h/\partial n) \quad \text{(Eq 21)}$$

in which

$$\partial h/\partial n = (h_w - h)/d_w \quad \text{(Eq 22)}$$

Table 1 List of boundary conditions applied

S_Cathode	
ϕ	$d\phi/dn = 0$
Ai	$dAi/dn = 0$
h	$h = h_{2000K}$
Cathode tip	
ϕ	$j(r)$
Ai	$dAi/dn = 0$
h	$h = h_{3600K}$
Sext_Anode	
ϕ	$\phi = 0$
Ai	$dAi/dn = 0$
T	Convection or $dT/dn = 0$
Inlet	
ϕ	$d\phi/dn = 0$
Ai	$dAi/dn = 0$
h	$h = h_{288K}$
Outlet	
ϕ	$d\phi/dn = 0$
Ai	$Ai = 0$
h	$dh/dn = 0$

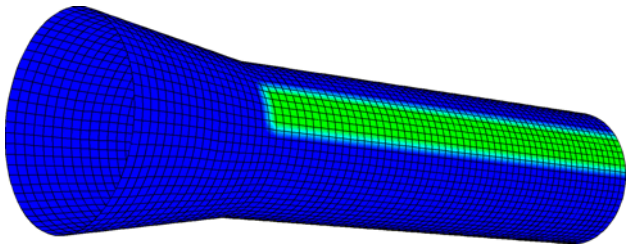

Fig. 2 View of the artificial electrical conductive layer applied over the anode surface

h_w and d_w being the values of the plasma enthalpies at the T_w temperature, and the distance from the cell center to the wall, respectively, and h being the in-cell value of the enthalpy.

The use of this equation to calculate the heat flux at the anode wall has now been found to provide an underestimation of thermal losses and a subsequent overestimation of the torch efficiency for given parameters. It could be changed in future works to account for the energy released by the electrons entering the anode material (Ref 22, 23, 27), but this modification has not been implemented yet.

3. Numerical Results

The case of an argon/hydrogen plasma gas mixture (35/10 slpm, respectively) with an electric arc current intensity of 600 A was considered.

The predicted temperature field is presented in Fig. 3 The plasma flow presents a very high temperature core just downstream the cathode tip: the temperature remains higher at 25 K over an axial extend of 20 mm. The arc attachment over the anode is privileged along the conductive line.

The corresponding pressure field is presented in Fig. 4. Because of the use of a compressible model, the overpressure at the cathode tip may be taken into account. The upstream value of the calculated pressure is about 0.017 MPa, whereas the maximum pressure found just

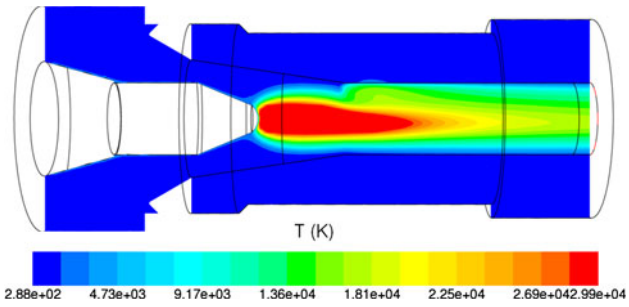

Fig. 3 Computed temperature field obtained for the 3D-coupled model

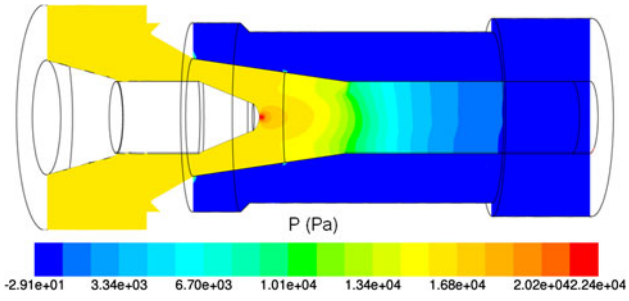

Fig. 4 Computed pressure field obtained for the 3D-coupled model

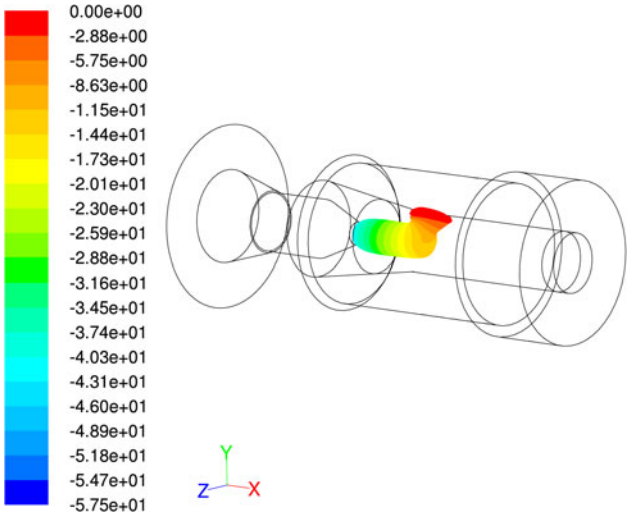

Fig. 5 Electric potential field over the $j = 20\ \mathrm{A \cdot mm^{-2}}$ iso-surface

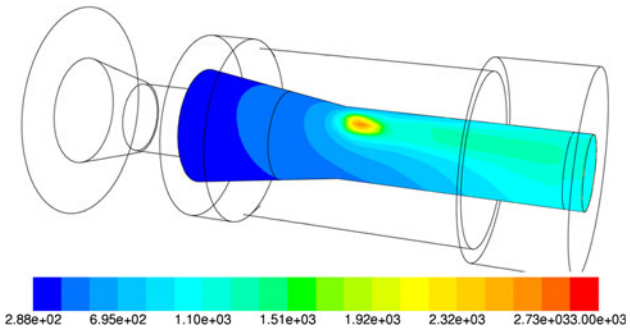

Fig. 6 Computed surface temperature of the anode

downstream the cathode tip is 0.022 MPa. Finally, the pressure field obtained for the 3D model looks very similar to that calculated for the 2D simulation (Ref 3).

The electric potential is shown in Fig. 5 over the iso-surface of constant current density $j = 20\ \mathrm{A \cdot mm^{-2}}$. This iso-surface is almost cylindrical just downstream the cathode tip and includes a root connecting the hot core of the plasma to the anode surface. The electric potential is comprised between 0 V at the anode surface and −57.5 V at the cathode tip.

The computed surface temperature of the anode in presented in Fig. 6. The ability of a model to predict such data is something new according to our knowledge (some noncoupled models may also provide this type of data by considering an effective thermal resistance between the internal surface and the cooling water circuit). The maximum temperature at the arc root attachment point is about 2500 K and the surface temperature increases downstream (i.e., the ending part of the anode seems to be its hottest part). The average surface temperature of the tungsten part (central zone) is 790 K (about 520 °C), whereas the average surface temperature of the copper part (one region left and a 2 mm long zone at the right) is about 210 °C. Concerning the mass averaged temperature values, they are about 480 °C for the tungsten part and 400 °C for the copper part.

The integral over the plasma volume of the ohm heating term Q_J represents about 32 kW for the 3D model, which remains below the experimental value (about 37.5 kW for these parameters). The radiative loss term contribution was computed to be about −1.7 kW whereas the contribution of the last term of the enthalpy equation ($\vec{V} \cdot \vec{\nabla} P$) was −0.52 kW only (cooling effect as for the radiative loss term).

The predicted torch voltage obtained for the 3D model is higher than for the 2D case but remains below the reality (39.3 V for the 2D model against 53.3 V for the 3D one and about 62.5 V for the experimental value).

However, the major discrepancy is that the thermal power transferred to the anode remains underestimated, whatever the method used to estimate it:

$$\int_{\text{Sanode}} \frac{\kappa}{Cp} \frac{(h - h_w)}{d_w} \mathrm{d}S \approx 4.5\ \mathrm{kW} \qquad \text{(Eq 23)}$$

and

$$\int_{\text{Sanode}} \kappa \frac{(T - T_w)}{d_w} \mathrm{d}S \approx 7.3\ \mathrm{kW} \qquad \text{(Eq 24)}$$

The thermal flux balance at the cathode tip was found to be more satisfactory (2.8 or 2.4 kW depending on the method).

Concerning the temperature values at the outlet section, the surface integrated value $\frac{1}{S}\int_S T\,\mathrm{d}s$ is about 9600 K. However, according to the model, the temperature presents a sharp profile at the nozzle axis with a quite cold temperature region surrounding the core of the plasma.

4. Conclusions

This article was devoted to the study of the plasma flow through the new ProPlasma HP gun from Saint-Gobain Coating Solutions (Avignon, France). A 3D stationary model was developed to compute the main characteristics of the plasma flow. The model implements a fluid/solid coupling in which the electromagnetic equations are solved not only in the plasma but also in the solid regions of the computational domain (tungsten and copper parts of the anode). In particular, it allows estimating the average value of the anode surface temperature and the average temperatures of the tungsten and copper parts. The ability of a model to provide this type of results is something new according to our knowledge. However, since the power transferred to the anode and evacuated by the water circuit is underestimated, a particular attention will have to be paid to the thermal exchanges mechanisms between the arc and the anode. The second main advance compared to previous works, concerns the fact that the calculation domain includes all upstream components of

the gun, such as the gas injection sleeves. It is thus possible to consider easily the case of straight or swirl-type injectors. Finally, the model remained stationary in the presented results, but the objective is to make it transient once it will be well established.

References

1. J. Zierhut, P. Haslbeck, K.D. Landes, G. Barbezat, M.Muller, and M. Schutz, TRIPLEX—An Innovative Three Cathode Plasma Torch, *Thermal Spray: Meeting the Challenges of the 21st Century*, C. Coddet, Ed., ASM International, 1998, p 1375-1379
2. F.A. Muggli, R.J. Molz, R. McCullough, and D. Hawley, Improvement of Plasma Gun Performance using Comprehensive Fluid Element Modeling Part I, *J. Therm. Spray Technol.*, 2007, **16**(5-6), p 677-683
3. R. Bolot, M.P. Planche, C. Coddet, A. Allimant, and D. Billières, *CFD Modeling of the Flow through the New ProPlasma HP Gun*, Rencontres Internationales de Projection Thermique, Lille (France), 2010
4. A.B. Murphy and P. Kovitya, Mathematical Model and Laser-Scattering Temperature Measurements of Direct-Current Plasma Torch Discharging into Air, *J. Appl. Phys.*, 1993, **73**(10), p 4759-4769
5. X. Chen and H.P. Li, Heat Transfer and Fluid Flow in a High Intensity Free-Burning Arc: An Improved Modelling Approach, *Int. J. Heat Mass Transf.*, 2001, **44**, p 2541-2553
6. S.W. Chau, K.L. Hsu, D.L. Lin, J.S. Chen, and C.C. Tzeng, Modeling and Experimental Validation of a 1.2 MW DC Transferred Well-Type Plasma Torch, *Comput. Phys. Commun.*, 2007, **177**, p 114-117
7. H.P. Li and X. Chen, Three-Dimensional Modelling of a DC Non-Transferred Arc Plasma Torch, *J. Phys. D Appl. Phys.*, 2001, **34**, p L99-L102
8. P.J. Bhuyan and K.S. Goswami, Two-Dimensional and Three-Dimensional Simulation of DC Plasma Torches, *IEEE Trans. Plasma Sci.*, 2007, **35**(6), p 1781-1786
9. B. Selvan, K. Ramachandran, K.P. Sreekumar, T.K. Thiyagarajan, and P.V. Ananthapadmanabhan, Numerical and Experimental Studies on DC Plasma Spray Torch, *Vacuum*, 2010, **84**, p 444-452
10. M.P. Planche, Z. Duan, O. Lagnoux, J. Heberlein, P. Fauchais, and E. Pfender, Study of Arc Fluctuations with different Plasma Spray Torch Configurations, *Proceedings of the 13th International Symposium on Plasma Chemistry*, Vol III, C.K. Wu, Ed., 1997 (Beijing, China), p 1460-1465
11. M.P. Planche, J.F. Coudert, and P. Fauchais, Velocity Measurements for Arc Jets Produced by a DC Plasma Spray Torch, *Plasma Chem. Plasma P*, 1998, **18**(2), p 263-283
12. J.L. Dorier, M. Gindrat, C. Hollenstein, A. Salito, M. Loch, and G. Barbezat, Time-Resolved Imaging of Anodic Arc Root Behavior During Fluctuations of a DC Plasma Spraying Torch, *IEEE Trans. Plasma Sci.*, 2001, **29**(3), p 494-501
13. Z. Duan and J. Heberlein, Arc Instabilities in a Plasma Spray Torch, *J. Therm. Spray Technol.*, 2002, **11**(1), p 44-51
14. J.F. Bisson, B. Gauthier, and C. Moreau, Effect of Plasma Fluctuations on In-Flight Particle Parameters, *J. Therm. Spray Technol.*, 2003, **12**(1), p 38-43
15. J.F. Bisson and C. Moreau, Effect of Direct-Current Plasma Fluctuations on In-Flight Particle Parameters: Part II, *J. Therm. Spray Technol.*, 2003, **12**(2), p 258-264
16. E. Nogues, M. Vardelle, P. Fauchais, and P. Granger, Arc Voltage Fluctuations: Comparison Between Two Plasma Torch Types, *Surf. Coat Technol.*, 2008, **202**, p 4387-4393
17. J.P. Trelles, E. Pfender, and J. Heberlein, Multiscale Finite Element Modeling of Arc Dynamics in a DC Plasma Torch, *Plasma Chem. Plasma Process.*, 2006, **26**, p 557-575
18. J.P. Trelles and J.V.R. Heberlein, Simulation Results of Arc Behavior in Different Plasma Spray Torches, *J. Therm. Spray Technol.*, 2006, **15**(4), p 563-569
19. E. Moreau, C. Chazelas, G. Mariaux, and A. Vardelle, Modeling the Restrike Mode Operation of a DC Plasma Spray Torch, *J. Therm. Spray Technol.*, 2006, **15**(4), p 524-530
20. J.P. Trelles, C. Chazelas, A. Vardelle, and J.V.R. Heberlein, Arc Plasma Torch Modeling, *J. Therm. Spray Technol.*, 2009, **18**(5-6), p 728-752
21. J.J. Gonzalez, P. Freton, and A. Gleizes, Comparisons Between Two- and Three-Dimensional Models: Gas Injection and Arc Attachment, *J. Phys. D Appl. Phys.*, 2002, **35**, p 3181-3191
22. F. Lago, J.J. Gonzalez, P. Freton, and A. Gleizes, A Numerical Modelling of an Electric Arc and Its Interaction with the Anode: Part I. The Two-Dimensional Model, *J. Phys. D Appl. Phys.*, 2004, **37**, p 883-897
23. C. Baudry, A. Vardelle, G. Mariaux, M. Abbaoui, A. Lefort, and E. Meillot, Numerical Modeling of a DC Non-Transferred Plasma Torch: Movement of the Arc Anode Attachment and Resulting Anode Erosion, *High Temp. Mater. Process.*, 2005, **9**, p 1-15
24. R. Bolot, ''Modélisation des Ecoulements de Plasmas d'Arc Soufflé: Application à la Projection de Matériaux Pulvérulents (Modeling of DC Plasma Flows: Application to Thermal Spray of Powder Materials),'' PhD Thesis, University of Franche-Comté (France), (in French), 1999
25. A. Deiber and O. Kempf, Lampe à Incandescence Corps Noir, loi de Stefan et Filtre Passe-Bas Thermique, *Bull. Union Phys. (in French)*, 2000, **827**(94), p 1595-1624
26. A.T.M. Wilbers, J.J. Beulens, and D.C. Schram, Radiative Energy Loss in a Two-Temperature Argon Plasma, *J. Quant. Spectrosc. Ratiat. Transf.*, 1991, **46**, p 385-392
27. F. Lago, ''Modélisation de l'Interaction entre un Arc Electrique et une Surface: Application au Foudroiement d'un Aéronef,'' PhD thesis, Toulouse (France), (in French), 2004